Article

Researching the Variation of Typhoon Intensities Under Climate Change in Vietnam: A Case Study of Typhoon Lekima, 2007

Tran Quoc Lap[ID]

Faculty of Water Resource Engineering, Thuyloi University, 175 Tay Son, Dong Da, Hanoi 10000, Vietnam; lapwru.edu@gmail.com or tranquoclap@tlu.edu.vn

check for updates

Abstract: Most of the typhoons that impact coastal regions of Vietnam occur from the north to the central part, between June and November. As a result of global warming, typhoon intensities are expected to increase. Therefore, an assessment of various typhoon strengths is essential. In this study, Typhoon Lekima, which hit Vietnam in 2007, was simulated by weather research and forecast models, using ensemble simulation methodology. Reproductive results of the typhoon intensity are similar to actual estimated values from the Japan Meteorological Agency. Also, the variation of typhoon intensities and heavy rainfall in future climate scenarios was investigated using numerical simulations based on pseudo global warming conditions, constructed using fifth-phase results of the Coupled Model Intercomparison Project multi-model global warming experiments. Simulation results of five Pseudo Global Warming (PGW_FF) models indicate that intensities of the typhoon will be magnified in future climate. The minimum sea level pressure of typhoons similar to Typhoon Lekima in the future will increase from 8 hPa to 9 hPa, and the spatial distribution of maximum wind speed and tracked direction will move towards the southern regions. Total precipitation will significantly increase for a maximum of six hours, and the spatial distribution of heavy rain caused by typhoons will shift from the north to the southwest of Vietnam. In the future, simulated results showed that global warming correlates strongly with a significant increase in typhoon intensity and heavy rain.

Keywords: climate change; numerical simulation; typhoon; ensemble simulation; pseudo global warming

1. Introduction

Climate change has become a topic of much concern in recent years. Besides global warming patterns, the possible change in tropical cyclone intensity is also a matter of great concern to the public and scientists. One of the significant concerns about the consequences of 21st-century climate change is the increase in typhoon intensity. Many studies have attempted to predict future climate change associated with warmer sea surface temperature (SST) using increased CO2 scenarios, global circulation models (GCMs) and regional climate models. Most of the studies projected a future increase in tropical cyclone (TC) intensity from +2 to +11% globally [1–7]. Vecchi et al. noted that Atlantic hurricane power dissipation is also well-correlated with other SST indices besides tropical Atlantic SST alone [8]. Using the downscaling Climate Model Intercomparison Project (CMIP) models, Emanuel et al. (2008) and Emanuel (2013) showed increased tropical cyclone activity in the western North Pacific and North Atlantic over the course of the 21st century [9,10]. Zhang et al. found that under global warming, the TC track density and power dissipation index (PDI) both exhibited robust and pronounced increasing trends over the North Pacific basin [11]. Current models have also projected a

reduced frequency of TCs globally, with a wide range of predictions among models, ranging from 6 to 34% reduction by the late 21st century. In individual ocean basins, these models project that the frequency may either increase or decrease by a substantial percentage [1,7,12–21]. However, scientists have low confidence in projected changes in tropical storm activity in individual ocean basins. There is some agreement that it is likely that the global frequency of tropical cyclones will either decrease or remain essentially unchanged in response to 21st-century climate warming [6,10,19,22].

Tropical storms tend to be larger and more intense in the western North Pacific (WNP) basin than in any other ocean basin [23]. The typhoons that make landfall on the coasts of Vietnam or Southern China originate near the Philippines in the South China Sea. Some agencies, such as the Hong Kong Observatory and the Regional Specialized Meteorological Center in Tokyo, monitor the development, movement and strength of typhoons in the WNP, and keep historical records of past storms. Every year, there is an average of five to six typhoons affecting the coastal area of Vietnam. Most of the typhoons occur from the north to the central region of Vietnam. The typhoon season usually lasts from June to November, with the highest frequency in September. Sometimes, it may begin as early as March and last until December.

When typhoons move in over land, they can cause severe damage, often resulting in human and economic losses. There are many examples of typhoons leaving an enormous number of casualties behind. For example, Typhoon Cecil in 1985 caused the deaths of 900 people, and Typhoon Dan in 1989 killed 352 people [24]. Typhoons with strong wind cause severe damage, quickly destroying poorly constructed houses and other structures. As a result, it is important to predict the variation of typhoon intensities, in term of minimum sea level pressure (MSLP), maximum wind speed (MWS), and the spatial distribution of rainfall, as accurately as possible.

In this study, the pseudo global warming (PGW_FF) downscaling approach [25] was applied. The primary goal of this paper is to investigate the future change in intensity of typhoons and heavy rainfall in the coastal area of Vietnam. For this purpose, authors selected Typhoon Lekima in 2007, and conducted reproductive and pseudo global warming (PGW_FF) experiments to investigate the intensity changes of the typhoon. Typhoon Lekima was the most destructive storm over this area in the 2000s, and it caused a heavy loss of human lives and huge damages to properties in Vietnam and Lao PDR due to storm surge, strong wind, and heavy rainfall.

In Section 2, an overview of the dataset and design of the dynamic downscaling (DDS) with PGW forcing data is provided. In Section 3, simulated results of control runs (CTL) and PGW_FF experiments on Typhoon Lekima are discussed. Finally, a summary is given in Section 4.

2. Data and Methodology

2.1. Data

2.1.1. Japanese 55-Year Reanalysis (JRA-55)

The Japan Meteorological Agency (JMA) started the second Japanese global atmospheric reanalysis project, named the Japanese 55-year Reanalysis (JRA-55). It covers 55 years, extending back to 1958 when the global radiosonde observing system was established. Many of the deficiencies found in the first Japanese reanalysis, the Japanese 25-year Reanalysis (JRA-25), were improved. JRA-55 aims at providing a comprehensive atmospheric dataset that is suitable for studies of climate change or multi-decadal variability, by producing a more time-consistent dataset for a longer period than JRA-25.

The Japanese 55-year reanalysis product (JRA-55) by the Japan Meteorological Agency (JMA) was used for simulations of the heavy rain event in 2008. JRA-55 was produced by a system based on the low-resolution (TL319) version of the JMA's operational data assimilation system, which has been extensively improved since the previous reanalysis (JRA-25). The atmospheric component of JRA-55 was based on the incremental four-dimensional variational method. Newly available and improved past observations are used for JRA-55. Major problems in JRA-25 (cold bias in the lower

stratosphere and dry bias in the Amazon) were resolved in JRA-55; therefore, the temporal consistency of temperature was improved. Further details are available in Kobayashi et al. [26].

2.1.2. Climate Model Intercomparison Project (CMIP5)

Global warming experiments, namely, the Climate projections of the fifth phase of the Climate Model Intercomparison Project (CMIP5), were used for the preparation of the PGW conditions. In CMIP5 (Taylor et al. 2012) [27], simulations of climate projections were conducted according to several greenhouse gas emission scenarios, i.e., representative concentration pathways (RCPs). For example, in the RCP4.5 scenario, the radiative forcing of the Earth becomes 4.5 W/m^2 by the end of the 21st century (Taylor et al. 2012) [27]. In this study, projections based on the RCP4.5 scenario were used, details of which are presented in Table 1.

Table 1. List of the Climate Model Intercomparison Project (CMIP5) models used in the research.

CMIP5_ID	Ensemble Name	Institute	Country
CanESM2	PGW_FF_1	Canadian Centre for Climate Modelling and Analysis	Canada
CNRM_CM5	PGW_FF_2	Centre National de Recherches Meteorologiques/Centre Europeen de Recherche et Formation Avancees en Calcul Scientifique	France
HadGEM2-CC	PGW_FF_3	Met Office Hadley Centre (additional HadGEM2-ES realizations contributed by Instituto Nacional de Pesquisas Espaciais	United Kingdom
MIROC-ESM	PGW_FF_4	Geophysical Fluid Dynamics Laboratory, USA	United States
MRI-CGCM3	PGW_FF_5	Japan Agency for Marine-Earth Science and Technology, Atmosphere and Ocean Research Institute (The University of Tokyo), and National Institute for Environmental Studies	Japan

2.1.3. Sea Surface Temperature (SST)

The National Oceanic and Atmospheric Administration (NOAA) $\frac{1}{4}°$ daily Optimum Interpolation Sea Surface Temperature (or daily OISST) is an analysis constructed by combining observations from different platforms (satellites, ships, buoys) on a regular global grid. A spatially complete SST map is produced by interpolating to fill in gaps.

The methodology included a bias adjustment of satellite and ship observations (referenced to buoys) to compensate for platform differences and sensor biases. This proved critical during the Mt. Pinatubo eruption in 1991, when the widespread presence of volcanic aerosols resulted in infrared satellite temperatures that were much cooler than actual ocean temperatures (Reynolds et al. 2007) [28]

For SST in the simulations, we used the NOAA Optimum Interpolation 1/4 Degree Daily Sea Surface Temperature Analysis (NOAA OI SST) [28]. The NOAA OI SST dataset has a grid resolution of 0.25° and a temporal resolution of one day. The product uses Advanced Very High-Resolution Radiometer infrared satellite SST data. Advanced Microwave Scanning Radiometer SST data were used after June 2002. In situ data from ships and buoys were also used for the large-scale adjustment of satellite biases.

2.1.4. Land-Surface Conditions

In this study, we used National Centers for Environmental Prediction (NCEP) data. These NCEP FNL (Final) Operational Global Analysis data are on 1-degree by 1-degree grids, prepared operationally

every six hours. This product is from the Global Data Assimilation System (GDAS), which continuously collects observational data from the Global Telecommunications System (GTS), and other sources, for many analyses. The FNLs are made with the same model that NCEP uses in the Global Forecast System (GFS), but the FNLs are prepared about an hour or so after the GFS is initialized. The FNLs are delayed so that more observational data can be used. The GFS is run earlier in support of time-critical forecast needs, and uses the FNL from the previous 6-h cycle as part of its initialization. The data spatial resolution is $1.0° \times 1.0°$ (NCEP 2000) [29].

The analyses are available on the surface, at 26 mandatory (and other pressure) levels from 1000 millibars to 10 millibars, in the surface boundary layer and at some sigma layers, the tropopause and a few others. Parameters include surface pressure, sea level pressure, geopotential height, temperature, sea surface temperature, soil values, ice cover, relative humidity, u- and v-winds, vertical motion, vorticity, and ozone.

2.1.5. Rainfall Data for Verification

As rainfall data for the verification of the Lekima results, we used in situ observation data from seven rain gauge stations in the coastal regions of Vietnam. In Vietnam, weather radar stations over the whole territory are fairly sparse. Hence, to examine the detailed distribution of precipitation in the central region of Vietnam, simulated results were compared with the APHRODITE precipitation dataset (Asian Precipitation—Highly-Resolved Observational Data Integration towards Evaluation). The APHRODITE dataset Ver.1101R2, with a spatial resolution of 0.25° for the Monsoon Asia region, was used in this study (Yatagai et al. 2012) [30].

2.1.6. Overview of Tropical Cyclone Lekima

A tropical depression formed in the South China Sea at 06:00 UTC 30 September 2007 at approximately 115° E/14.7° N. Initially, it moved in a northwest direction towards Hainan Island whilst simultaneously intensifying, before becoming a tropical storm named Lekima at 12:00 UTC, after which it continued in a northwest direction. Then, it slowly changed direction to west-northwest and continued getting stronger. At 00:00 UTC 02 October, it developed into a typhoon of category 3 on the Saffir–Simpson scale, continued its trajectory toward the Vietnamese coast, and hit land at 12:00 UTC 03 October at 106.5° E/17.9° N. The most dangerous aspects of storm Lekima were the very strong winds, coupled with heavy rainfall and flooding following its path. Total rainfall exceeded 400 mm at many observation sites, and the maximum value was 660 mm during 24 h in Thua Thin Hue Province.

The typhoon intensity datasets for calibrations of the Lekima results based on the Japan Meteorological Agency (JMA) are shown in Figure 1.
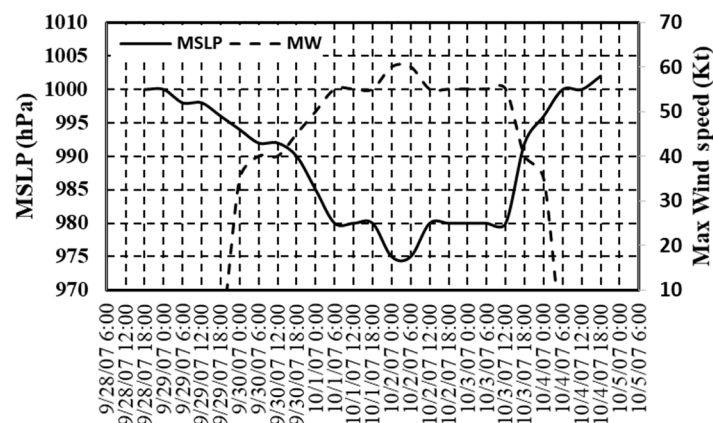

Figure 1. Minimum sea level pressure (MSLP) and maximum sustained wind speed of Typhoon Lekima in 2007.

2.2. Dynamical Downscaling Method

2.2.1. Pseudo Global Warming Conditions

Control simulations of Lekima (CTL) were performed with initial and boundary conditions prepared from JRA-55, NCEP FNL and NOAA 0.25 interpolated OI SST. In addition to CTL, we performed simulations with PGW forcing, prepared using different CMIP5 data. PGW conditions of Lekima were calculated from future and present climate conditions. The future weather conditions were obtained from the 10-year monthly mean from 2091 to 2100 with PGW_FF. Present climatic conditions were obtained from the 10-year monthly mean from 1991 to 2000, in historical simulation for CMIP5. Then, anomalies of global warming were calculated as the difference added to JRA-55. Thus, a set of PGW conditions was constructed for the wind, atmospheric temperature, geopotential height, surface pressure and specific humidity. For relative humidity, the original values in JRA-55 were retained in the PGW conditions, and specific humidity in these conditions was defined from the relative humidity and the modified atmospheric temperature of the future climate. To prepare SST for the PGW condition, the SST anomaly obtained from future and present climate conditions in the CIMP5 output was added to the NOAA SST.

2.2.2. Design of Numerical Simulations

In this study, the Weather Research and Forecasting model (WRF) version 3.6.1 was adopted for the CTL and PGW simulations. A two-way nesting grid system was used, as shown in Figure 2. The coarsest domain, D01, had a 30-km horizontal resolution, and the higher resolution domain, D02, had a 10-km horizontal resolution.
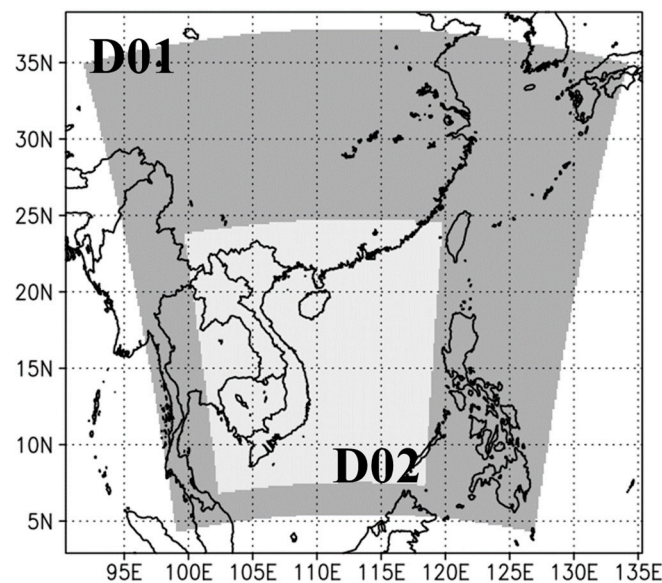

Figure 2. Target domains of downscaling in the Weather Research and Forecasting (WRF) model. The spatial resolutions are 30 km and 10 km for D01 and D02, respectively.

Ensemble simulations with different initial conditions were performed for the CTL and each PGW condition. At first, the lagged average forecast (LAF) method (Hoffman and Kalnay 1983) was used to obtain three different conditions: X_1, X_2, and X_3 (Figure 3). In LAF, multiple simulations with different initial times were performed. The three simulations were set up with 6-h lags so that the simulations began at 00:00 UTC, 06:00 UTC and 12:00 UTC on 30 September.
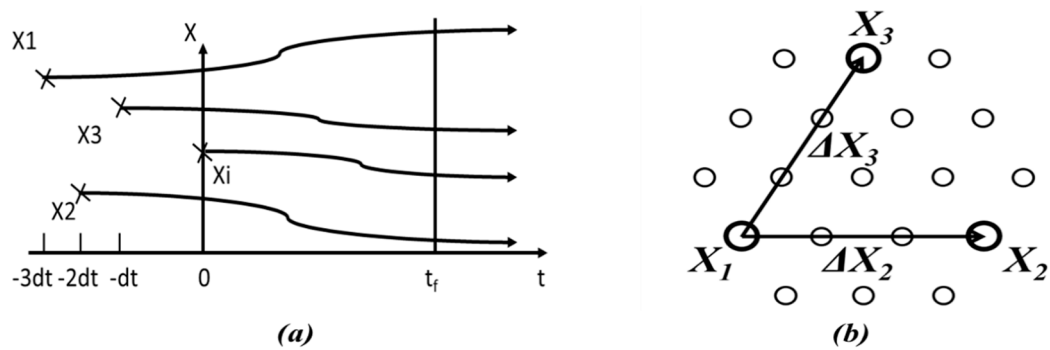
Figure 3. (**a**) Schematic view of the lagged average forecast (LAF) method, (**b**) ensemble member preparation. Large open circles are the base states (X_1, X_2, and X_3) made by the LAF method. Small open circles are newly prepared ensemble states.

From three ensemble members, two perturbation states (ΔX_2 and ΔX_3) were produced, as follows:

$$\Delta X_2 = X_2 - X_1 \tag{1}$$

$$\Delta X_3 = X_3 - X_1 \tag{2}$$

Then, a new state was made from the following equation:

$$X_n = X_1 + \alpha \times \Delta X_2 + \beta \times \Delta X_3 \tag{3}$$

Here, α and β are scale factors of ΔX_2 and ΔX_3. Sixteen new ensemble members were prepared at 00:00 UTC on 01 October. In total, 19 simulations were made (Figure 3) until 18:00 UTC 04 October. Pairs of the scale factors are listed in Table 2. Ensemble simulations enable the stochastic analysis of differences between CTL and PGW runs. Therefore, it could be determined whether differences were attributable to the effects of global warming or chaotic behaviors in the numerical weather model.

Table 2. Pairs of the scale factors (α and β).

(α, β)	(α, β)	(α, β)	(α, β)
(−1/3, 1/3)	(0, 2/3)	(1/3, 2/3)	(2/3, 1/3)
(−1/3, 2/3)	(1/3, −1/3)	(1/3, 1)	(2/3, 2/3)
(−1/3, 1)	(1/3, 0)	(2/3, −1/3)	(1, −1/3)
(0, 1/3)	(1/3, 1/3)	(2/3, 0)	(1, 1/3)

* The original three states (X_1, X_2, and X_3) are not included.

Kain–Fritsch cumulus parameterization (Kain 2004), and the microphysics parameterization schemes of Lin et al. (1983), were used in this study. Physical processes of the surface layer, land surface scheme, and planetary boundary layer scheme were computed by Fifth-Generation Penn State Mesoscale Model (MM5) similarity based on Moni–Obukhov with the Carlson Boland viscous sub-layer, the Noah Land Surface model (Chen et al. 2001), and the Yonsei University scheme (Hong et al. 2006). For longwave radiation, we used the Rapid Radiative Transfer Model (RRTM) scheme (Mlawer et al. 1997), and for shortwave radiation, we used the Goddard shortwave scheme (Chou and Suarez. 1994). For D01, a spectral nudging method was used for atmospheric temperature, zonal wind, meridional wind, and geopotential height every six hours at altitudes above 6–7 km. Model settings are given in Table 3.

Table 3. Settings in the Weather Research and Forecasting model.

Version of Model	V 3.6.1
Number of domain	Two
Horizontal grid distance	30 km (coarse domain); 10 km (fine domain)
Cloud microphysics	Lin et al. method
Cumulus parameterization	Kain–Fritsch scheme cumulus parameterization
Longwave radiation	RRTM scheme (Rapid Radiative Transfer Model)
Shortwave radiation	Goddard shortwave
Surface layer	MM5 similarity
Land surface scheme	Noah Land Surface model
Planetary boundary layer scheme	Yonsei University scheme
Setting of spectral nudging	A spectral nudging method was used for atmospheric temperature, zonal wind, meridional wind, and geopotential height every six hours, at altitudes above 6–7 km.

3. Results

3.1. Results of the CTL Run

Results of the CTL run are presented in Section 3.1 to assess typhoon Lekima intensities and, in comparison with observation data, in terms of MSLP at the center of the simulated typhoon, the maximum surface wind speed (MWS), the track of Typhoon Lekima, and heavy rainfall.

3.1.1. Minimum Sea Level Pressure, Maximum Wind Speed, and Tracks of the Typhoon

a. Minimum Sea Level Pressure

Figure 4 illustrates the time evolution of Typhoon Lekima intensity in terms of MSLP. It is clear that the simulation results of MSLP from nineteen ensemble members show that MSLP is higher than the estimated value from JMA in the first 60 h of typhoon Lekima, from 06:00 UTC 01 October to 18:00 UTC 03 October. However, after typhoon Lekima made landfall on 12:00 UTC 03 October, the observed MSLP was higher than the simulated values. For instance, at 18:00 UTC 03 October, observed MSLP of JMA was 992.5 hPa, compared to 987 hPa average of simulation values from nineteen ensemble members. The observed values show that the power dissipation of the storm from 980 to 1000 hPa was faster than the simulated results. The highest difference between a simulated value and an estimated value was 8 hPa, at 06:00 UTC 02 October. The comparison indicates that all simulations of central surface pressure agree well with the best-track data, through the intensification of the TC that occurred before its landfall in Vietnam was slightly delayed.

Figure 4 shows that from 06:00 UTC 01 October to 12:00 UTC 03 October the spatial correlation between the simulation results and observation data is stable and comparable. So, it can be used with the caveat of the direction of the tropical cyclone, for government and people, although the simulation results are overestimated when compared to observation data.

From 12:00 UTC 03 October, the time when tropical cyclone Lekima made landfall inland, the simulation results of MSLP were lower than the observation data, in this case, because the land-surface conditions used in this study, NCEP_FNL with a resolution of $1° \times 1°$, cannot cover the microphysics of the Truong Son mountain ridge that runs toward the southeast, with the width of the Truong Son mountain ridge from 30 km to 40 km being much smaller than the minimum considered by the NCEP_FNL dataset. So, it might not consider the peak of the Truong Son Mountain ridge (the Truong Son mountain peak is about 2300 m height above sea level), but rather treat it as flat terrain without the sudden change in topography. So, simulation results of MSLP gradually decreased inland due to a lack

of power, while the observation data of MSLP quickly decreased because the Truong Son mountain blocked the storm, as we can see in 12:00 UTC 03 October to 18:00 UTC 04 October (Figure 4).
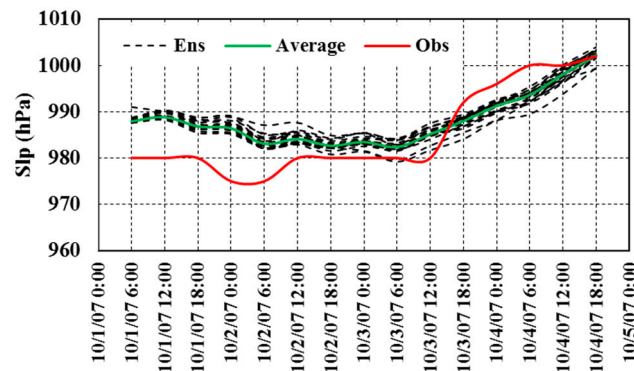

Figure 4. Estimated MSLP from nineteen ensemble members and observed MSLP from the Japan Meteorological Agency (JMA).

b. Maximum Wind Speed and Tracks

Figure 5a,b show the spatial distribution of MWS from JRA-55 data and simulated results of the model in the period from 06:00 UTC 01 October to 18:00 UTC 04 October. Authors recognize that the average value of wind speed from the CTL run tended to be stronger than JRA-55 and expanded from the north to the south, and from the sea to inland, during the typhoon in Vietnam.
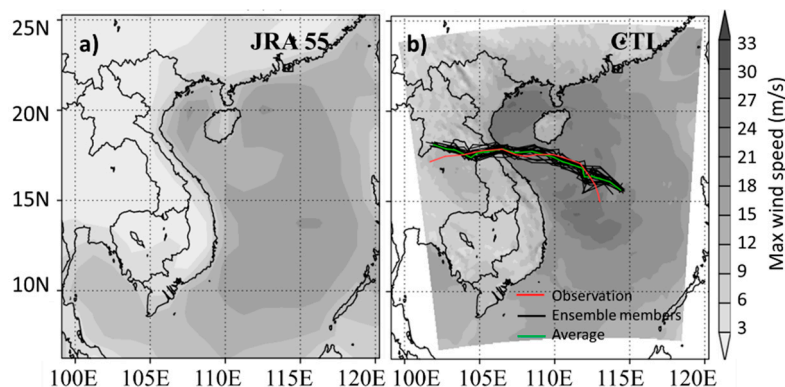
Figure 5. (**a**) Maximum wind speed (MWS) from the Japanese 55-year Reanalysis (JRA-55) dataset and (**b**) average MWS and track of typhoon Lekima simulated by WRF models, where the black line and green line each represent the average track of nineteen ensemble members, and the red line is the track observed by the JMA.

Figure 5b shows a comparison of predicted and JMA tracks using nineteen ensemble members in the D02 domain with 10 km spatial resolution. According to the JMA observations, typhoon Lekima was formed in the South China Sea at 06:00 UTC 30 September 2007 at approximately 114° E/14.7° N, and it moved in a northwest direction towards Hainan Island. However, the simulation results of nineteen ensemble members showed that the storm formed near 115° E and 15° N and moved to the northwest direction. The simulated tracks passed close to the track observed by the JMA, especially the average value from nineteen simulations (green line), not only in terms of the direction but also the location where typhoon Lekima made landfall (at 12:00 UTC 03 October 2007).

3.1.2. Rainfall

Figure 6 shows the spatial distribution of total precipitation from the APHRODITE dataset and an average of nineteen ensemble members of the CTL run. The results of the CTL run indicate that

the spatial distribution of heavy rainfall spread from the north to the south, and was concentrated mainly in the central region of Vietnam. The rainfall spatial distribution of the CTL run was similar to the APHRODITE dataset. However, the quantity of precipitation of the CTL run was higher than APHRODITE values.
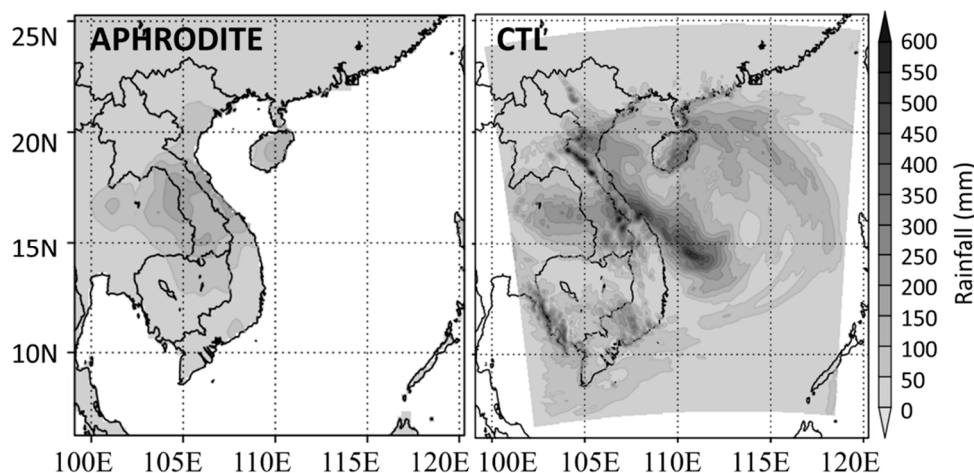

Figure 6.　Spatial distribution of heavy rain from 01 to 03 October, 2007 of Asian Precipitation—Highly-Resolved Observational Data Integration towards Evaluation (APHRODITE) data and a simulation of nineteen ensemble members.

3.2. Results of Pseudo Global Warming Experiments (PGW)

3.2.1. Minimum Sea Level Pressure, Maximum Wind Speed, and Track of Typhoon Lekima

a. Simulated Results of MSLP

From Figure 7, the multi-model ensemble experiment results, including the member in each model, show an increase in typhoon intensity. At 00:00 UTC 03 October, the average MSLP of 19 ensemble members simulated by the CTL run was 983.66 hPa, compared with 972.98 hPa and 979.2 hPa of PGW_FF_3 and PGW_FF_4, respectively. Meanwhile, the results of average MSLP of the 19 ensemble members simulated by the PGW_FF_1, PGW_FF_2, and PGW_FF_5 models are not much different from the results of the CTL run. Three PGW_FF experiments (PGW_FF_1, PGW_FF_2, and PGW_FF_5) simulating the future produced results for the MSLP of the typhoon that were similar to those of the CTL in the central region of Vietnam. Meanwhile, two PGW_FF experiments (PGW_FF_3 and PGW_FF_4) predicted that the MSLP would be lower than the results of the CTL run. Among ensemble members in each PGW_FF experiment, some similarities were found in MSLP. These results indicate that the effects of chaotic behaviors are expected to be small, the errors in initial conditions and in model physics result in forecast uncertainties. So, global warming mainly caused the difference between PGW_FF experiments and the CTL run. In this research, one approach for reducing these uncertainties is the use of ensemble forecasting. There was a wide variety in the MSLP among the nineteen ensemble members in the PGW_FF experiments and the CTL run. These results demonstrate the importance of ensemble simulations.
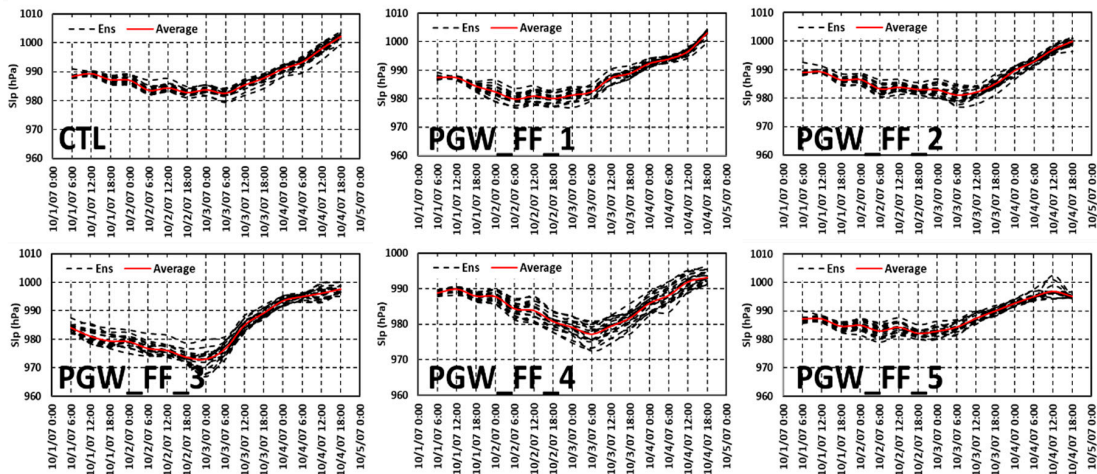
Figure 7. The predicted results from nineteen ensemble members of MSLP simulated by control (CTL) and PGW_FF experiments. Black dash lines and the red line are the results of each member and the average value of nineteen ensemble members, respectively.

b. Max Wind Speed and Tracks

The simulation results of the difference in MWP of Typhoon Lekima between CTL and PGW_FF experiments are shown in Figure 8. In PGW_FF_3 and PGW_FF_4 experiments, the MWS increased, strong wind was concentrated in the central region and tended to shift to the south over time. Meanwhile, the simulation results of PGW_FF_2 showed an increase in MWS in the offshore, before making landfall. PGW_FF_1 and PGW_FF_5 showed a slight decrease in MWS, compared with the CTL run. This may be caused by a difference in the location of landfall. In this case, the maximum wind speed would be affected by the Truong Son mountain ridge that runs toward the southeast, with the width of the Truong Son mountain from 30 km to 40 km and the peak about 2300 m in height. So, the simulation results of MWS decreased with the typhoon simulated by PGW_FF experiments with the same direction of CTL run.
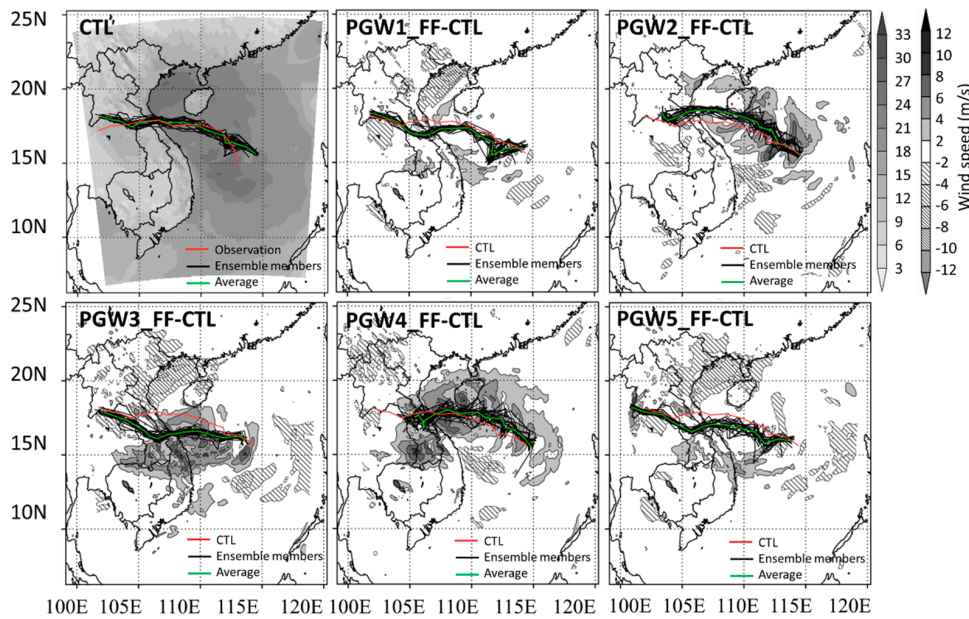

Figure 8. The average spatial distribution of MWS and the track of CTL, and different spatial distributions of average MWS between PGW_FF experiments with tracks from nineteen ensemble members of the typhoon, and the CTL run.

Figure 8 shows tracks in PGW_FF models with nineteen ensemble members. The simulated tracks of PGW_FF_1, PGW_FF_3, and PGW_FF_5 experiments moved to the southern regions of Vietnam, whereas in the PGW_FF_2 experiment, the typhoon tracks of ensemble members seemed to move in the direction of the northern area. The average track of PGW_FF_4 showed a similar tendency to the CTL run, however, it dissipated more quickly.

3.2.2. Simulation Results of Rainfall

a. The Magnitude of Rainfall

Figure 9 displays the relationship between maximum six-hourly rainfall and total rainfall from 00:00 UTC 01 October to 18:00 UTC 04 October of the CTL run and five PGW_FF models simulating the future. It is clear that both the maximum six-hourly and the total simulated rainfall show a strong increase compared with the simulated rainfall of the CTL run, except for the results of the PGW_FF_2 experiment, where simulated rainfall slightly decreased when compared with the CTL run. The highest increase in rainfall was seen in the results of the PGW_FF_3 experiment. Six-hourly and total rainfall from the nineteen ensemble members of the CTL run were 232.53 mm and 656.38 mm, rising to 426.46 mm and 1217.5 mm in PGW_FF_3, respectively. The simulated results from other models showed an increase from 18% to 76% in both six-hourly and total rainfall, when compared with the CTL run.
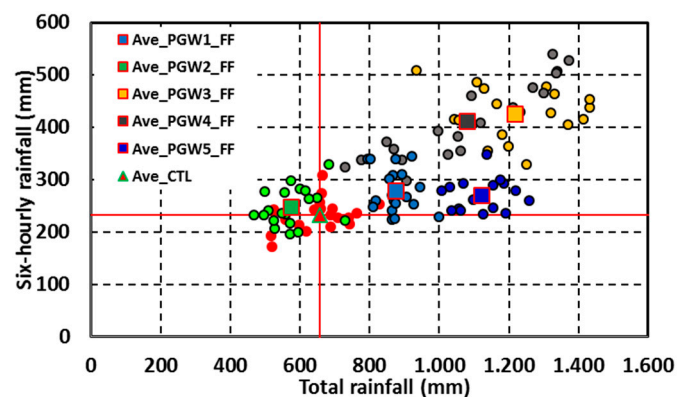

Figure 9. Simulation results of maximum six-hourly and total rainfall from 00:00 UTC 01 October to 18:00 UTC 04 October of the CTL runs and five PGWs models, in the future simulation in D02. The x-axis is total rainfall and the y-axis is maximum six-hourly rainfall. The unit is mm.

In this research, to assess the variation of total rainfall in the future, the authors used cumulative distribution curves (CDF) and assumed the normal distribution function. The results are shown in Figure 10.

Figure 10 presents CDF curves of average total rainfall simulated by PGW_FF experiments and the CTL run. It is clear that there was a significant increase in most of the PGW_FF experiments, except the CDF curve of PGW_FF_2.

Focusing on the probability of 75%, the results of CTL runs indicated that when a typhoon is similar to Typhoon Lekima in 2007, with a probability of total rainfall at 75%, the total rainfall from 00:00 UTC 01 October to 18:00 UTC 04 October will exceed 600 mm. On the other hand, the variation range of average total rainfall is from 720 mm to 1120 mm in most of the PGW_FF experiments. The maximum increase in rainfall comes from PGW_FF_3 simulations, with 1120 mm. However, the results of the PGW_FF_2 experiment showed a slight decrease in the total rain, with 410 mm and 530 mm, respectively. The increasing rainfall intensity in the future when simulated by five CMIP5 models could be explained by the fact that under global warming, water vapor in the atmosphere will be increased. At the same time, warmer SST will provide more water vapor. These are thought to be the main reasons for heavier rainfall in the future.
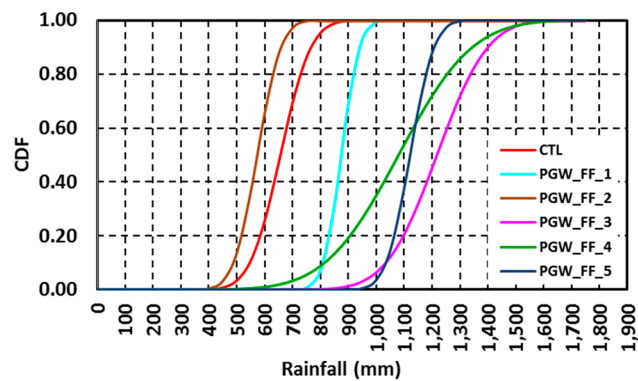
Figure 10. The cumulative distribution curves of average total rainfall from nineteen ensemble members simulated by PGW_FF experiments and the CTL run.

b. The Spatial Distribution of Heavy Rainfall

Figure 11 shows the spatial distribution of total rainfall from 00:00 UTC 01 October to 18:00 UTC 04 October of CTL runs and five PGW_FF experiments, in the future simulation in D02. The simulation results of the PGW_FF_3 and PGW_FF_4 models, when compared with the results of the CTL run, showed heavy rainfall areas covering the region from 14.5° N to 15.5° N and 104.5° E to 108.5° E. The rainfall spatial distribution occurred over a vast area, and it shifted from the north to the south and southwest, extending to Laos and Thailand. This rainfall could cause the severe flooding and landslides in the central region of Vietnam. Spatial distributions reflect a significant rise in rainfall in the future. However, in the PGW_FF_1 and PGW_FF_5 experiments, heavy rainfall decreased in the north and showed an increasing trend in the south of the central region, whereas, the spatial distribution of total rainfall as simulated by the PGW_FF_2 experiment showed a downward trend in heavy rainfall inland, with heavy rainfall concentrated over the South China Sea. The rain band may be affected by the location of the typhoon where it made landfall. These results are consistent with previous studies on the effect of climate change on the rainfall distribution caused by the typhoon [31].
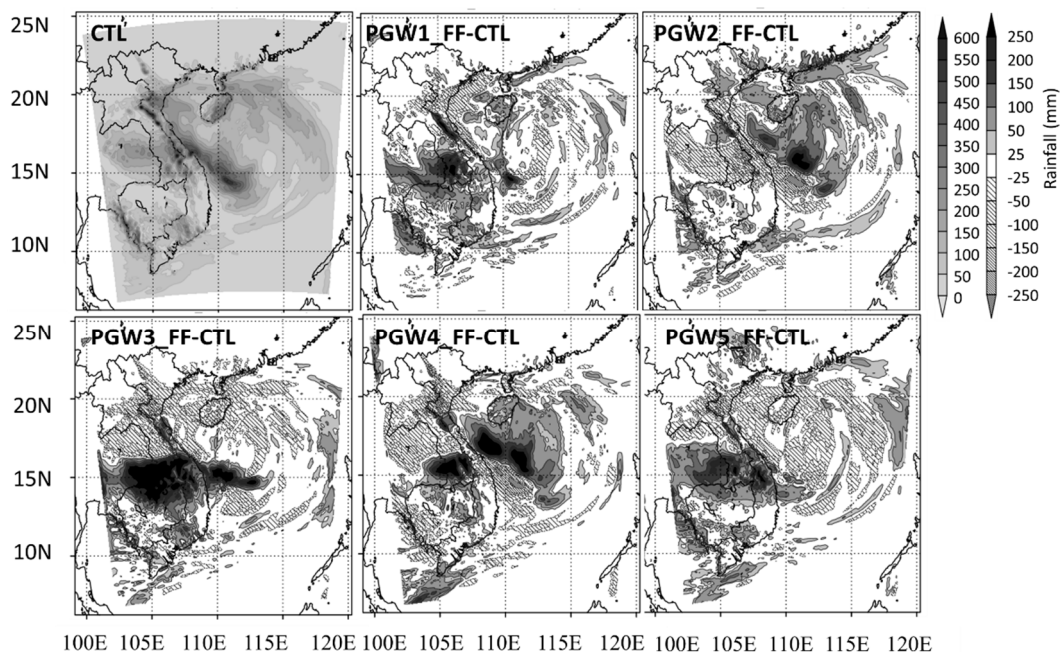

Figure 11. The average total rainfall spatial distribution of nineteen ensemble members of the CTL run, and the different spatial distribution of total rainfall between PGW_FF experiments and the CTL run.

In summary, total rainfall in the central regions of Vietnam caused by typhoons similar to Typhoon Lekima showed a projected increase in intensity in the future. The future spatial distribution of rainfall tended to shift from north to south and extended to Laos and Thailand. In the future, the results of rainfall simulated by PGW_FF_3 experiments showed the highest increase in intensity.

4. Conclusions

This study aims to perform a hindcast of typhoon Lekima, which hit the central region of Vietnam from 30 September to 04 October 2007, and calculates the variations in the intensity of Typhoon Lekima under global warming climate conditions, applying a downscaling approach to future projection from five CMIP5 models, using the PGW and ensemble methods.

In the hindcast and in each PGW_FF experiment, nineteen ensemble members were prepared by the LAF and ensemble methods to examine the differences between simulations caused by global warming. The simulation results of average MSLP from nineteen ensemble members were overestimated. At the time when typhoon Lekima made landfall in Vietnam, simulation results were slightly underestimated. This may be due to the effect of the Truong Son mountain ridge, when compared with the observation dataset of JMA. The spatial distribution of heavy rainfall caused by Typhoon Lekima shifted from north to south; however, the location and intensity are different among ensemble members.

In the future simulation with the PGW method, the typhoon intensity and total rainfall tend to increase when compared with the CTL run. When the typhoon made landfall, the simulated results of MSLP dropped in most models, and the spatial distribution of the MWS and the typhoon direction shifted to the southern region. The spatial distribution of total rainfall moved to the southwest to affect the central areas of Vietnam, Laos, and Thailand. The fluctuation range of rainfall, in six-hourly and total measurements, was wide among ensemble members of CTL runs and PGW_FF experiments. An increase in heavy rainfall could occur because, under global warming, saturated vapor will increase and the warm SST will provide more water vapor and moisture. So, we need to have more mechanisms of analysis. Furthermore, only one tropical cyclone was examined in this study to draw conclusions about variations in typhoon intensity due to future global warming, and this may include some degree of uncertainty.

Our results suggest that under global warming, a tropical cyclone similar to Lekima may bear more intensity and heavy rainfall in the future. The use of the PGW method and ensemble simulations can help governments and people living in the coastal region to understand more about the variation of typhoon intensities, especially the increase in heavy rainfall, which is the main cause of flooding in Central Vietnam.

References

1. Knutson, T.R.; Tuleya, R.E. Impact of CO_2-induced warming on simulated hurricane intensity and precipitation: Sensitivity to the choice of climate model and convective parameterization. *J. Clim.* **2004**, *17*, 3477–3495. [CrossRef]
2. McDonald, E.R.; Bleaken, D.G.; Cresswell, D.R.; Pope, V.D.; Senior, C.A. Tropical storms: Representation and diagnosis in climate models and the impacts of climate change. *Clim. Dyn.* **2005**, *25*, 19–36. [CrossRef]
3. Chauvin, F.; Royer, J.F.; Deque, M. Response of hurricane-type vortices to global warming as simulated by arpege-climat at high resolution. *Clim. Dyn.* **2006**, *27*, 377–399. [CrossRef]

4.　Oouchi, K.; Yoshimura, J.; Yoshimura, H.; Mizuta, R.; Kusunoki, S.; Noda, A. Tropical cyclone climatology in a global-warming climate as simulated in a 20kmmesh global atmospheric model: Frequency and wind intensity analyses. *J. Meteorol. Soc. Jpn.* **2006**, *84*, 259–276. [CrossRef]

5.　Knutson, R.; Coauthors, T. Tropical cyclones and climate change. *Nat. Geosci.* **2010**, *3*, 157–163. [CrossRef]

6.　Emanuel, K.; Oouchi, K.; Satoh, M.; Tomita, H.; Yamada, Y. Comparison of explicitly simulated and downscale tropical cyclone activity in a high-resolution global climate model. *J. Adv. Model. Earth Syst.* **2010**, *2*, 9. [CrossRef]

7.　Bengtsson, L.; Hodges, K.I.; Esch, M.; Keenlyside, N.; Kornblueh, L.; Luo, J.J.; Yamagata, T. How may tropical cyclones change in a warmer climate? *Tellus* **2007**, *59A*, 539–561. [CrossRef]

8.　Vecchi, G.A.; Swanson, K.L.; Soden, B.J. Climate change: Whither hurricane activity? *Science* **2008**, *322*, 687–689. [CrossRef]

9.　Emanuel, K.A. Downscaling cmip5 climate models shows increased tropical cyclone activity over the 21st century. *Proc. Natl. Acad. Sci. USA* **2013**, *110*, 12219–12224. [CrossRef]

10.　Emanuel, K.; Sundararajan, R.; Williams, J. Hurricanes and global warming: Results from downscaling ipcc ar4 simulations. *Bull. Am. Meteorol. Soc.* **2008**, *89*, 347–367. [CrossRef]

11.　Zhang, L.; Karnauskas, K.B.; Donnelly, J.P.; Emanuel, K. Response of the north pacific tropical cyclone climatology to global warming: Application of dynamical downscaling to cmip5 models. *J. Clim.* **2017**, *30*, 1233–1243. [CrossRef]

12.　Broccoli, A.K.; Manabe, S. Can existing climate models be used to study anthropogenic changes in tropical cyclone climate? *Geophys. Res. Lett* **1990**, *17*, 1917–1920. [CrossRef]

13.　Haarsma, R.J.; Mitchell, J.F.; Senior, C.A. Tropical disturbances in a gcm. *Clim. Dyn.* **1993**, *8*, 247–257. [CrossRef]

14.　Bengtsson, L.; Botzet, M.; Esch, M. Will greenhouse gas-induced warming over the next 50 years lead to higher frequency and greater intensity of hurricanes? *Tellus* **1996**, *48A*, 57–73. [CrossRef]

15.　Krishnamurti, T.N.; CORREA-TORRES, R.I.C.A.R.D.O.; Latif, M.; Daughenbaugh, G. The impact of current and possibly future sea surface temperature anomalies on the frequency of atlantic hurricanes. *Tellus* **1998**, *50A*, 186–210. [CrossRef]

16.　Royer, J.-F.; Chauvin, F.; Timbal, B.; Araspin, P.; Grimal, D. A gcm study of the impact of greenhouse gas increase on the frequency of occurrence of tropical cyclones. *Clim. Chang.* **1998**, *38*, 307–343. [CrossRef]

17.　Tsutsui, J. Implications of anthropogenic climate change for tropical cyclone activity: A case study with the ncar CCM2. *J. Meteorol. Soc. Jpn.* **2002**, *80*, 45–65. [CrossRef]

18.　Yoshimura, J.; Sugi, M.; Noda, A. Influence of greenhouse warming on tropical cyclone frequency. *J. Meteorol. Soc. Jpn.* **2006**, *84*, 405–428. [CrossRef]

19.　Zhao, M.; Held, I.M.; Lin, S.-J.; Vecchi, G.A. Simulations of global hurricane climatology, interannual variability, and response to global warming using a 50-km resolution gcm. *J. Clim.* **2009**, *22*, 6653–6678. [CrossRef]

20.　Knutson, T.R.; Sirutis, J.J.; Garner, S.T.; Vecchi, G.A.; Held, I.M. Simulated reduction in atlantic hurricane frequency under twenty-first-century warming condition. *Nat. Geosci.* **2008**, *1*, 359. [CrossRef]

21.　Nguyen, K.-C.; Walsh, K.J.E. Interannual, decadal, and transient greenhouse simulation of tropical cyclone-like vortices in a regional climate model of the south pacific. *J. Clim.* **2001**, *14*, 3043–3054. [CrossRef]

22.　Sugi, M.; Murakami, H.; Yoshimura, J. A reduction in global tropical cyclone frequency due to global warming. *Sola* **2009**, *5*, 164–167. [CrossRef]

23.　Chavas, D.R.; Emanuel, K.A. A quikscat climatology of tropical cyclone size. *Geophys. Res. Lett.* **2010**, *37*, L18816. [CrossRef]

24.　Quynh, D.N.; Ninh, P.V.; Manh, V.M.; Lien, N.T.V. The typhoon surges in vietnam: The regime characteristics and prediction. In *5th Asean Science and Technology Week*; Center for Marine Environment, Survey, Research, Consultation: Hanoi, Vietnam, 1998; pp. 178–194.

25.　Sato, T.; Kimura, F.; Kitoh, A. Projection of global warming onto regional precipitation over mongolia using a regional climate model. *J. Hydrol.* **2007**, *333*, 144–154. [CrossRef]

26.　Kobayashi, S.; Ota, Y.; Harada, Y.; Ebita, A.; Moriya, M.; Onoda, H.; Onogi, K.; Kamahori, H.; Kobayashi, C.; Endo, H.; et al. The jra-55 reanalysis: General specifications and basic characteristics. *J. Meteorol. Soc. Jpn* **2015**, *93*, 5–48. [CrossRef]

27. Taylor, K.E.; Stouffer, R.J.; Meehl, G.A. An overview of cmip5 and the experiment design. *Bull. Am. Meteorol. Soc.* **2013**, *93*, 485–498. [CrossRef]

28. Reynolds, R.W.; Smith, T.M.; Liu, C.; Casey, K.S.; Schlax, M.G. Daily high-resolution blended analysis for sea surface temperature. *J. Clim.* **2007**, *20*, 5473–5496. [CrossRef]

29. NCEP. Ncep fnl operational model global tropospheric analyses, continuing from july 1999. In *Research Data Archive at the National Center for Atmospheric Research, Computational and Information Systems Laboratory*; NCEP: Boulder, CO, USA, 2000.

30. Yatagai, A.; Kamiguchi, K.; Arakawa, O.; Hamada, A.; Yasutomi, N.; Kitoh, A. Aphrodite: Constructing a long-term daily gridded precipitation dataset for asia based on a dense network of rain gauges. *Bull. Am. Meteorol. Soc.* **2012**, *93*, 1401–1415. [CrossRef]

31. Tran, L.Q.; Taniguchi, K. Simulations of heavy rainfall from a tropical cyclone in coastal regions of vietnam under the global warming. *J. Clim. Chang.* **2016**, *2*, 25–34. [CrossRef]